Original Article

DOI: 10.5582/bst.2024.01121

A predictive radiotranscriptomics model based on DCE-MRI for tumor immune landscape and immunotherapy in cholangiocarcinoma

Lu Chen[1,6,§], Guotao Yin[2,§], Ziyang Wang[3,4,6,§], Zifan Liu[3,6], Chunxiao Sui[3,6], Kun Chen[3,6], Tianqiang Song[1,6], Wengui Xu[3,6], Lisha Qi[5,6,*], Xiaofeng Li[3,6,*]

[1] Department of Hepatobiliary Cancer, Liver Cancer Research Center, Tianjin Medical University Cancer Institute and Hospital, Tianjin, China;
[2] Department of Radiology, Qilu Hospital of Shandong University, Jinan, Shandong, China;
[3] Department of Molecular Imaging and Nuclear Medicine, Tianjin Medical University Cancer Institute and Hospital, Tianjin, China;
[4] Department of Nuclear Medicine, Tianjin Cancer Hospital Airport Hospital, Tianjin, China;
[5] Department of Pathology, Tianjin Medical University Cancer Institute and Hospital, Tianjin, China;
[6] National Clinical Research Center for Cancer, Tianjin Key Laboratory of Cancer Prevention and Therapy, Tianjin's Clinical Research Center for Cancer, Tianjin, China.

SUMMARY This study aims to determine the predictive role of dynamic contrast-enhanced magnetic resonance imaging (DCE-MRI) derived radiomic model in tumor immune profiling and immunotherapy for cholangiocarcinoma. To perform radiomic analysis, immune related subgroup clustering was first performed by single sample gene set enrichment analysis (ssGSEA). Second, a total of 806 radiomic features for each phase of DCE-MRI were extracted by utilizing the Python package Pyradiomics. Then, a predictive radiomic signature model was constructed after a three-step features reduction and selection, and receiver operating characteristic (ROC) curve was employed to evaluate the performance of this model. In the end, an independent testing cohort involving cholangiocarcinoma patients with anti-PD-1 Sintilimab treatment after surgery was used to verify the potential application of the established radiomic model in immunotherapy for cholangiocarcinoma. Two distinct immune related subgroups were classified using ssGSEA based on transcriptome sequencing. For radiomic analysis, a total of 10 predictive radiomic features were finally identified to establish a radiomic signature model for immune landscape classification. Regarding to the predictive performance, the mean AUC of ROC curves was 0.80 in the training/validation cohort. For the independent testing cohort, the individual predictive probability by radiomic model and the corresponding immune score derived from ssGSEA was significantly correlated. In conclusion, radiomic signature model based on DCE-MRI was capable of predicting the immune landscape of chalangiocarcinoma. Consequently, a potentially clinical application of this developed radiomic model to guide immunotherapy for cholangiocarcinoma was suggested.

Keywords chalangiocarcinoma, DCE-MRI, radiotranscriptomics, tumor immune landscape, immunotherapy

1. Introduction

Cholangiocarcinoma is the second most common primary liver malignancy after hepatocellular carcinoma (HCC) worldwide, accounting for approximately 10%–20% of all primary liver cancers (*1*). Increasing evidences show that its morbidity and mortality rates have steadily risen in the past decades (*2*). Despite tremendous progress in advanced treatment, the prognosis of cholangiocarcinoma patients remains dismal, with a 5-year overall survival (OS) rate ranging from 14% to 40% (*3*). Because most of cholangiocarcinoma patients are already in the advanced clinical stage with the occurrence of early invasion and metastasis at the time of original diagnosis, which leads to minor eligibility for surgical resection (*4*), development of novel treatment strategies for cholangiocarcinoma is urgently needed.

Currently, immunotherapy is emerging as a promising therapeutic strategy for various types of cancers (*5*). Particularly with the clinical application of immune checkpoint blockade (ICB) treatment in a couple of types of cancer, including melanoma (*6*), lymphoma (*7*) and non-small cell lung cancer (NSCLC) (*8*), tumor immunotherapy has revolutionized the management

of cancer patients in recent decades. As reviewed in an updated report regarding immunotherapy for cholangiocarcinoma, several novel immunotherapeutic approaches, such as adoptive cell transfer therapy, cancer vaccines and ICB treatment combined with other targeted therapy, are currently under investigation (*9,10*). Unfortunately, only 20-50% of patients with advanced solid tumors significantly benefit from ICB therapy, mainly due to intrinsic heterogeneity in tumor (*11*). Therefore, it is of necessity to identify robust predictive biomarkers for selection of potentially responsive patients prior to immunotherapy (*12,13*).

Previous reports proved predictive roles of tumor immune landscape in tumor immunotherapy, reflected in a remarkably significant association between the status of tumor-infiltrating lymphocytes (TILs) (*14*) or programmed death-ligand 1 (PD-L1) (*15*) in tumor microenvironment (TME) and therapeutic efficacy to ICB treatment. However, tumor immunophenotype is currently assessed by immunohistochemistry (IHC) assay (*16*) and flow cytometric analyses, which mainly depends on biopsy specimen availability. Given the complexity of the staining procedure, lack of standardization and subjectivity of results interpretation and the spatio-temporal heterogeneity in tumorous tissues, a noninvasive, repeatable and reliable method is urgently needed to overcome these deficiencies. Dynamic contrast-enhanced magnetic resonance imaging (DCE-MRI) is one of the most commonly used imaging modalities in clinical practice for cholangiocarcinoma (*17*). Apart from conventional parameters based on MRI images, radiomic analysis and deep learning algorithms based on MRI images also exhibited a predictive power in prediction of tumor immune status for multiple types of cancer, including cholangiocarcinoma (*18,19*).

Radiomics, emerging as a novel technique, allows for a high-throughput analysis to extract the hidden non-visual features and establish corresponding descriptive or predictive models to characterize the intrinsic heterogeneous nature of tumors reflected in medical images (*20*). However, with the rapid development of radiomics, the biological rationale underlying the high predictive power of established radiomic models is increasingly required, which is not only an important tendency but also a challenge for radiomic studies in future (*21*). Radiomics combined with genomics or associated transcriptomics is significantly helpful to reintroduce biological meaning into radiomics. That was the very reason why we chose to perform radiotranscriptomics but not traditional radiomics in the study. Though TIL score and/or PD-1/PD-L1 status is predictive of the tumor immune landscape, a comprehensive characterization of the tumor immunophenotype is needed to substantially improve the prospect of tumor immunotherapy. With the development of next-generation sequencing techniques and the rise of bioinformatic analysis, distinct immune subtypes in the TME of cholangiocarcinoma were characterized based on transcriptome sequencing, representing the comprehensive tumor immune landscape (*22,23*).

For radiotranscriptomics in the present investigation, transcriptomic signature was used as a starting point to identify the predictive imaging radiomic signature. In other words, tumor immune subgroups classification for cholangiocarcinoma was first achieved based on transcriptome sequencing data by an unsupervised clustering method. Then, quantitative radiomic features were extracted and selected to establish a potentially predictive radiomic signature model for tumor immune subgroups classification in cholangiocarcinoma. Finally, the predictive power of this developed radiomic signature model was evaluated by the value of area under the curve (AUC) based on receiver operating characteristic (ROC) analysis. Furthermore, cholangiocarcinoma patients with immunotherapy who underwent transcriptome sequencing after surgery and DCE-MRI examination prior to treatment were also included as an independent testing cohort to test the potential of this model in prediction of immunotherapy. Promisingly, this constructed radiomic signature model based on DCE-MRI was able to noninvasively and comprehensively characterize the local tumor immune landscape, and then guide immunotherapy for cholangiocarcinoma in clinical practice.

2. Materials and Methods

2.1. Patients selection

All recruited patients eligible for this present investigation met the following strict criteria: (1) patients with biopsy-proven diagnosis of cholangiocarcinoma after surgical resection; (2) patients who underwent preoperative liver DCE-MRI within 1 month of surgery; (3) patients without preoperative adjuvant treatment, such as chemotherapy, radiotherapy, molecular targeted therapy and other treatment; (4) patients who underwent specimen transcriptome sequencing and IHC staining for immune cells infiltration. The exclusion criteria were as follows: (1) patients without complete clinicopathologic information; (2) patients without qualified MRI images for tumor segmentation; (3) patients without valid sample transcriptome sequencing data or tumoral IHC assay results. A total of 365 cholangiocarcinoma patients were screened to recruit eligible candidates who underwent preoperative DCE-MRI examination and postoperative transcriptome sequencing. Among cholangiocarcinoma candidates undergoing transcriptome sequencing after surgery (n = 72), cholangiocarcinoma patient with complete preoperative DCE-MRI information (n = 44) was used as traing cohort (n = 34) (3-fold cross-validation, 50 repeation) and independent testing cohort (n = 10) to construct and evaluate a preliminay radiotranscriptomics model for

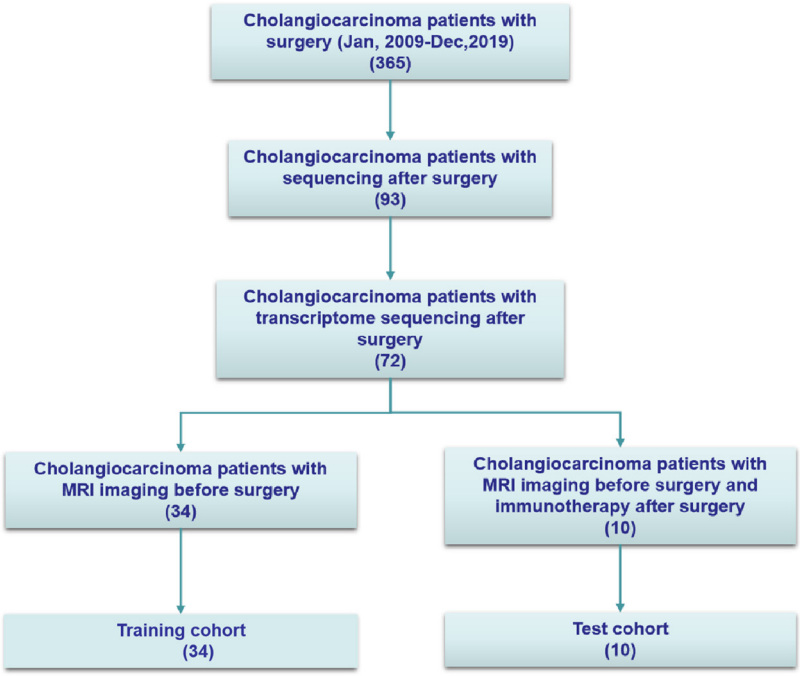

Figure 1. The flowchart of cholangiocarcinoma patients' enrollment in the study.

immunotherapy. The inclusion and exclusion flowchart for the patient enrollment in the study is represented in Figure. 1. The clinicopathological characteristics of these included cholangiocarcinoma patients based on immune-related subgroup clustering are summarized in Table 1. This retrospective study was approved by the our institutional ethics review committee (EK20240068), and the written informed consent requirement was waived because of the retrospective nature of this study. This study conforms to the provisions of the Declaration of Helsinki (as revised in 2013) and the provisions of the ICMJE recommendations and the CONSORT 2010 guidelines.

2.2. MRI acquisition

All MR examinations were performed by using a 3.0-T whole-body MRI system (Discovery MR750; GE Medical Systems, Milwaukee, WI) equipped with a quadrature body coil. Axial dynamic contrast-enhanced magnetic resonance imaging (DCE-MRI) (3D liver acquisition with volume acceleration-extended volume, LAVA-XV) consisted of non-contrast agent-enhanced, arterial phase (20-35 seconds), portal phase (60 seconds), 3-minute transitional phase and 20-minute delayed hepatobiliary phase images. The contrast agent, gadolinium diethylenetriaminepentaacetic acid (Gd-DTPA; Bayer Healthcare, Berlin, Germany) (0.1 mmol/kg), was automatically administered intravenously at the second phase of the DCE-MRI protocol at 2 mL/sec by using a power injector system, followed by a 20 mL saline flush at the same rate. These images were obtained using a breath-hold T1-weighted three-dimensional with fat suppression fast spoiled gradient echo sequence. Repetition time/echo time (TR/TE) = 4/1.8 ms, number of excitations: (NEX) = 0.7, bandwidth = 142.9 kHz, thickness = 4mm, slice gap = -2mm, field of view (FOV) = 26 cm, matrix = 220×192, flip angle (FA) = 12°.

2.3. Immunotherapy and transcriptome sequencing for cholangiocarcinoma

A total of 10 advanced cholangiocarcinoma patients with postoperative transcriptome sequencing data were enrolled for immunotherapy in combination with systematic chemotherapy in the present investigation. Sintilimab were administered intravenously at a dose of 3 mg/kg every 3 weeks for at least 4 courses of treatment until disease progression or unacceptable toxic events. Therapy response was evaluated by radiological assessment (using computed tomography or magnetic resonance imaging) at baseline and then every 12 weeks during treatment or follow-up. The primary endpoint was the proportion of patients with disease control at week 12, including complete response (CR), partial response (PR), stable disease (SD) and progressive disease (PD) according to Response Evaluation Criteria In Solid Tumors (RECIST) v1.1 criteria. CR, PR and SD were categorized into the "clinical benefit (CB)" group, whereas PD was categorized into the "non-clinical benefit (NCB)" group for immunotherapy response evaluation. For transcriptome sequencing, each well-preserved fresh frozen block was first used to isolate Ribonucleic Acid (RNA) using the RNeasy Mini Kit (Qiagen) according to the manufacturer's instruction. After the construction of RNA-sequencing (RNA-seq) libraries using NEBNext Ultra RNA Library (New England Biolabs), 150-bp paired-end reads were checked for quality and sequenced

Table 1. Clinicopathologic characteristics of cholangiocarcinoma patients included in the study

Parameters	Immune-related classification		*P*
	Subgroup 1 (*n* = 17), *n* (%)	Subgroup 2 (*n* = 17), *n* (%)	
Location			0.29
ICC	9 (52.9)	12 (70.6)	
ECC	8 (47.1)	5 (29.4)	
Gender			0.72
Female	6 (35.3)	7 (41.2)	
Male	11 (64.7)	10 (58.8)	
Age (year)			
< 60	7 (41.2)	8 (47.1)	0.73
≥ 60	10 (58.8)	9 (52.9)	
Tumor size (cm)			0.78
< 3	6 (35.3)	8 (47.1)	
≥ 3 < 5	4 (23.5)	3 (17.6)	
≥ 5	7 (41.2)	6 (35.3)	
Lesion number			1.00
One	16 (94.1)	16 (94.1)	
More than one	1 (5.9)	1 (5.9)	
Differentiation			0.89
Low	1 (5.9)	2 (11.8)	
Medium-low	9 (52.9)	7 (41.2)	
Medium	6 (35.3)	7 (41.2)	
High	1 (5.9)	1 (5.9)	
Perineural invasion			0.99
Absence	13 (76.5)	13 (76.5)	
Presence	4 (23.5)	4 (23.5)	
Vascular invasion			0.99
Absence	14 (82.4)	15 (88.2)	
Presence	3 (17.6)	2 (11.8)	
Lymph node metastasis			0.99
Absence	15 (88.2)	14 (82.4)	
Presence	2 (11.8)	3 (17.6)	
CEA (μg/L) median (IQR)	2.48 (1.41-3.49)	2.53 (1.57-2.81)	0.94
CA199 (U/ml) median (IQR)	6.07 (14.62-331.03)	45.59 (22.77-214.90)	0.91
TBIL (μmol/L) median (IQR)	13.00 (10.35-77.90)	23.30 (12.00-68.03)	0.30
DBIL (μmol/L) median (IQR)	2.70 (1.73-36.18)	6.35 (2.33-34.50)	0.25
HBV infection			0.99
Absence	13 (76.5)	14 (82.4)	
Presence	4 (23.5)	3 (17.6)	
AJCC 8th TNM			0.98
I	8 (47.1)	9 (52.9)	
II	5 (29.4)	4 (23.5)	
III	3 (17.6)	3 (17.6)	
IV	1 (5.9)	1 (5.9)	
$CD3^+$ T infiltration			**0.002**
High	13 (76.5)	4 (23.5)	
Low	4 (23.5)	13 (76.5)	
$CD8^+$ T infiltration			**0.02**
High	12 (70.6)	5 (29.4)	
Low	5 (29.4)	12 (70.6)	
$FOXP3^+$ T infiltration			**0.04**
Positive	5 (29.4)	0 (0)	
Negative	12 (70.6)	17 (100)	

ICC: Intrahepatic cholangiocarcinoma; ECC: Extrahepatic cholangiocarcinoma; CEA: Carcinoma Embryonic Antigen; CA199: Carbohydrate antigen 199; HBV: Hepatitis B virus; HCV: Hepatitis C virus; TBIL: Total bilirubin; DBIL: Direct bilirubin; AJCC: American Joint Committee on Cancer; CD3/4/8: Cluster of differentiation 3/4/8; FOXP3: Forkhead box protein 3; IQR: Interquartile range.

with Illumina Novaseq (Illumina).

2.4. Immune-related subgroup clustering for cholangiocarcinoma based on transcriptome sequencing data

First, RNA-sequencing data from the included cholangiocarcinoma patients were first standardized for further analysis. Then, immune-related subgroup clustering for cholangiocarcinoma was performed by using gene set enrichment analysis (GSEA) and the K-means algorithm. Briefly, a total of 29 immune-associated gene sets were chosen to represent tumor immunity as previously reported by literature, and the gene set variation analysis (GSVA) package was used for

single sample gene set enrichment analysis (ssGSEA) of the 29 immune gene sets. K-means algorithm, a classical unsupervised learning algorithm of artificial intelligence, was used for subgroup clustering in R software version 3.6.0 (*https://www.r-project.org/*) by 50 iterations. The total within the sum of square and average silhouette width was calculated using R package factoextra to determine the optimal number of clustering. Afterwards, the ConsensusClusterPlus package in R software was used for consensus clustering and subgroup screening of ssGSEA scores. In addition, a principal component analysis (PCA) plot was also drawn to verify the reliability of the consensus clusters. In the end, the heatmap package in R software was used for heatmap visualization of the ssGSEA scores for the aforementioned 29 immune gene sets based on subgroup clustering to illustrate the distinct immune characteristics of different subgroups.

2.5. Immunohistochemical analysis for the tumor-infiltrating lymphocytes in cholangiocarcinoma

Streptavidin-biotin-peroxidase staining was performed to determine the immune landscape in the tumorous tissue of cholangiocarcinoma. Briefly, paraffin embedding slides were first deparaffinized, rehydrated and pretreated with microwaves and blocking according to typical protocols. Then, the slides were incubated with a series of primary antibodies against several immunological markers overnight at 4°C according to the manufacturer's instructions, including CD3, CD8 and FOXP3. Finally, signals on the slides were revealed using 3,3-diaminobenzidine (DAB) buffer as substrate after incubation with appropriate horseradish peroxidase (HRP)-conjugated secondary antibodies (1:2000; Santa Cruz Biotechnology, Inc., Dallas, TX) for 1 hour at room temperature. Three most independent and representative fields in tissues for each case were selected and photographed (×200 magnification) to evaluate the levels of T lymphocyte infiltrations with an Olympus digital camera. Then, the numbers of infiltrating lymphocytes in each field were automatically and recorded as previously described (*24*) using Image pro plus 6.0 software (Media Cybernetics Inc.). The averages of infiltration were calculated and used for statistical analysis.

2.6. Radiomics workflow

The radiomics workflow in the study mainly consists of (1) Lesion segmentation, (2) radiomic features extraction, (3) radiomic features reduction and selection; (4) radiomic signature/model construction and clinical use. The detailed workflow of the radiotranscriptomics is schemed in Figure. 2. The 3D Slicer version 4.10.2 (open-source software; *https://www.slicer.org/*) was used for semiautomatic segmentation. The volume of interest (VOI) segmentation and subsequent radiomic features extraction for each lesion were performed in a blinded fashion by two radiologists with > 10 years' experience (reader 1 and reader 2) based on multiple images per phase of DCE-MRI, and only indicator lesion was delineated if multiple lesions existed. Radiomic features extraction was performed by utilizing open-source Python package Pyradiomics 1.2.0 (*http://www.radiomics.io/pyradiomics.html*). Both original features and wavelet features were extracted in the study. A total of 806 radiomic features were generated for each VOI based on per phase of MRI, including shape features, first-order statistic features, second-order features, higher-order statistic features and wavelet features. Radiomic features reduction and selection were performed to select the most informative features to construct radiomic models. In the present investigation, three steps were adopted to avoid or reduce overfitting and selection bias. Firstly, the intra-class coefficients (ICCs) with a threshold of 0.95 were used to select the stable features that were not easily affected by the process of delineation. Then, spearman correlation analysis with a Spearman correlation coefficient of 0.75 was performed to reduce the redundancy between selected radiomic features. Third, the Man-Whitney *U* test ($p < 0.05$) was used to identify the informative radiomic features that significantly differ between the two immune-related subgroups. Lastly, a support vector machine with rbf kernel was employed to establish the radiomic model. Due to the limited sample size, three-fold cross-validation was performed and repeated 50 times in the training set. Furthermore, the calibration performance was also evaluated by the Hosmer-Lemeshow test. To test the predictive power of the established radiomic model in immune related subgroup classification and immunotherapy, another 10 cholangiocarcinoma patients with ICB treatment were recruited as an independent testing cohort.

2.7. Statistical analysis

For all continuous variables, normal distribution and variance homogeneity were first assessed. Those with a normal distribution were expressed as mean and standard deviation (mean ± SD), while those with non-normal distributions were expressed as medians and interquartile range. The inter-group statistical differences for numerical variables were determined by the *t*-test (normal distribution), the Mann-Whitney *U* test/ or Wilcoxon Rank Sum tests (non-normal distribution), while the chi-square test or Fisher's exact test was used for categorical variables. Inter-observer agreement was used to assess the reliability of the MRI evaluation using the Kappa test, and the performance of the developed radiomic model based on DCE-MRI in immune profiling for cholangiocarcinoma was quantified by receiver operating characteristic (ROC) curve analysis and justified by the calibration curve. The area under the curve (AUC) of the ROC curve, classification accuracy, sensitivity

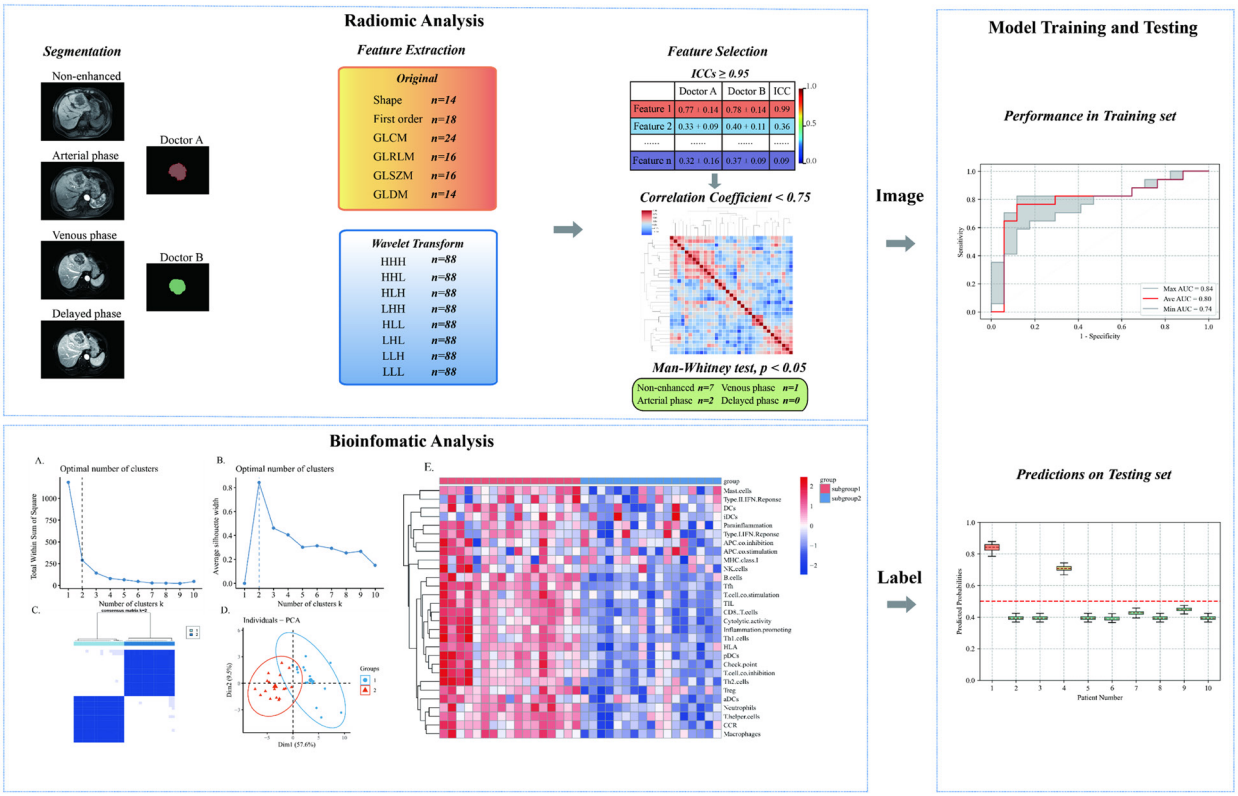

Figure 2. The detailed workflow of radiotranscriptomic analysis in the study. First, a bioinformatics analysis based on transcriptome sequencing data was performed to classify the immune-related subgroup, which was used as a label for subsequent radiomic analysis. Second, based on the label aforementioned, a radiomic analysis was conducted to establish a radiomic signature model, which mainly consists of VOI segmentation, radiomic features extraction, three-step features reduction and selection. Finally, a ROC analysis was performed to evaluate the power of the developed radiomic model in the prediction of immune landscape and immunotherapy for cholangiocarcinoma in both the training set and the testing set.

and specificity were also calculated by using Python (Version 3.6, *https://www.jianshu.com/p/b48d6bad9aaf*) for constructed radiomic model. The above statistical analyses were conducted using the software Python (Version 3.6, *https://www.jianshu.com/p/b48d6bad9aaf*) and IBM SPSS Statistics v. 20.0 (Armonk, NY). A P value of less than 0.05 is considered as statistically significant.

3. Results

3.1. Immune-related subgroup clustering for cholangiocarcinoma based on transcriptome sequencing data

For each included cholangiocarcinoma sample (n = 34), the gene set variation analysis (GSVA) package was used for single sample gene set enrichment analysis (ssGSEA) to obtain scores for a total of 29 immune-associated gene sets representing multiple immune cell types, functions and pathways. The K-means algorithm was used to determine the optimal cluster number. As shown in Figure. 3A and Figure. 3B, corresponding to both the turning point on the total within the sum of square (elbow method) and maximum average silhouette width (Silhouette Coefficient method), k = 2 was suggested as the optimal number of immune-related subgroup clustering for cholangiocarcinoma. The R package Consensus Cluster Plus was used to perform consensus matrix analysis for validation of the consensus clustering when k = 2 (Figure. 3C). Additionally, the principal component analysis (PCA) plots also showed the reliability of the consensus clusters based on the subgroup screening of ssGSEA scores (Figure. 3D). Ultimately, the distinct immune characteristics of the identified two subgroups were visualized in a heat map based on the ssGSEA scores for aforementioned 29 immune gene sets (Figure. 3E). As shown, the extent of immune cell infiltration in subgroup 1 was remarkably higher than that in subgroup 2 ($P < 0.05$).

3.2. Immune characteristics validation of the identified two immune-related subgroups

Based on the aforementioned immune-related subgroup clustering for cholangiocarcinoma, an IHC assay was performed to validate the differences in immune characteristics between the two subgroups. Consistent with the results illustrated in the heat map mentioned above, subgroup 1 was characterized by higher infiltrations for various types of immune cells compared to subgroup 2. As shown in the representative IHC images (Figure. 4A), for subgroup 1, which was considered as an immune-hot subtype, the densities of

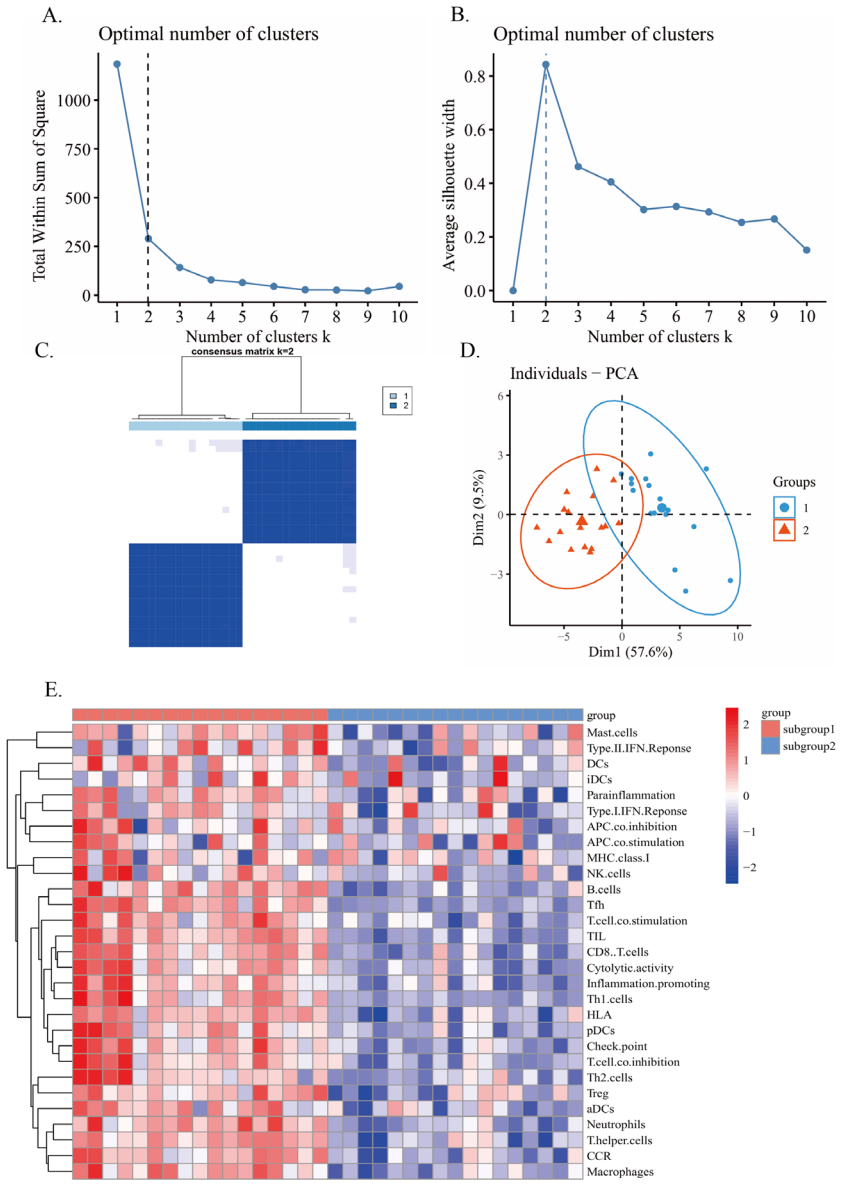

Figure 3. A bioinformatic analysis for immune-related subgroup clustering for cholangiocarcinoma recruited in the study based on transcriptome sequencing data. (**A**) The curve of the total within sum of squared error under corresponding cluster number k by using elbow method reached the "elbow point" when k = 2. (**B**) The curve of average silhouette width under corresponding cluster number k by using silhouette coefficient calculation, and the maximum of average silhouette width was achieved when k = 2. (**C**) The consensus clustering of immune-related subgroup of cholangiocarcinoma when k = 2. (**D**) The principal component analysis (PCA) plots of clustered samples of cholangiocarcinoma. (subgroup 1: blue; subgroup2: red). (**E**) The visualization of the distinct immune characteristics of the classified subgroups based on ssGSEA scores calculated by a GSVA package in the form of heat map.

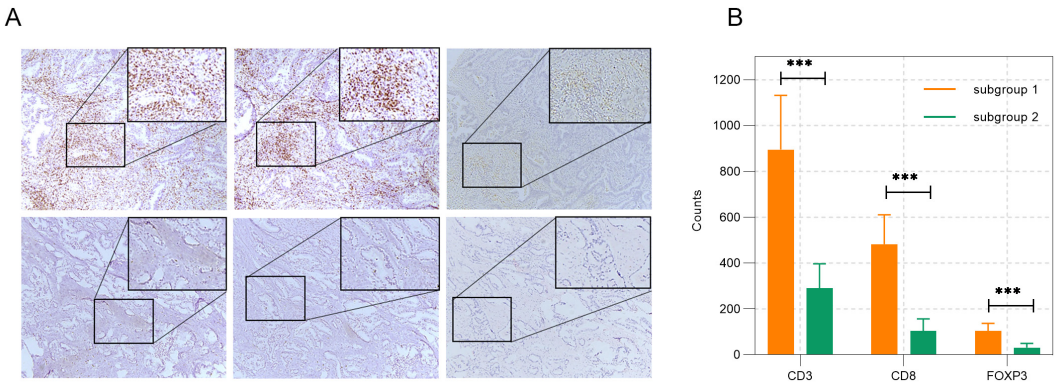

Figure 4. Validation of the immune-related subgroup clustering by IHC assay. (**A**) Representative IHC images of multiple immune cell infiltrations in cholangiocarcinoma for subgroup 1 (upper) and subgroup 2 (lower), including $CD3^+$ T (left), $CD8^+$ T (middle), and $FOXP3^+$ T cells (right). (**B**) The differences of $CD3^+$ T, $CD8^+$ T, and $FOXP3^+$ T cell infiltration in cholangiocarcinoma between subgroup 1 and subgroup 2 were summarized in the histogram.

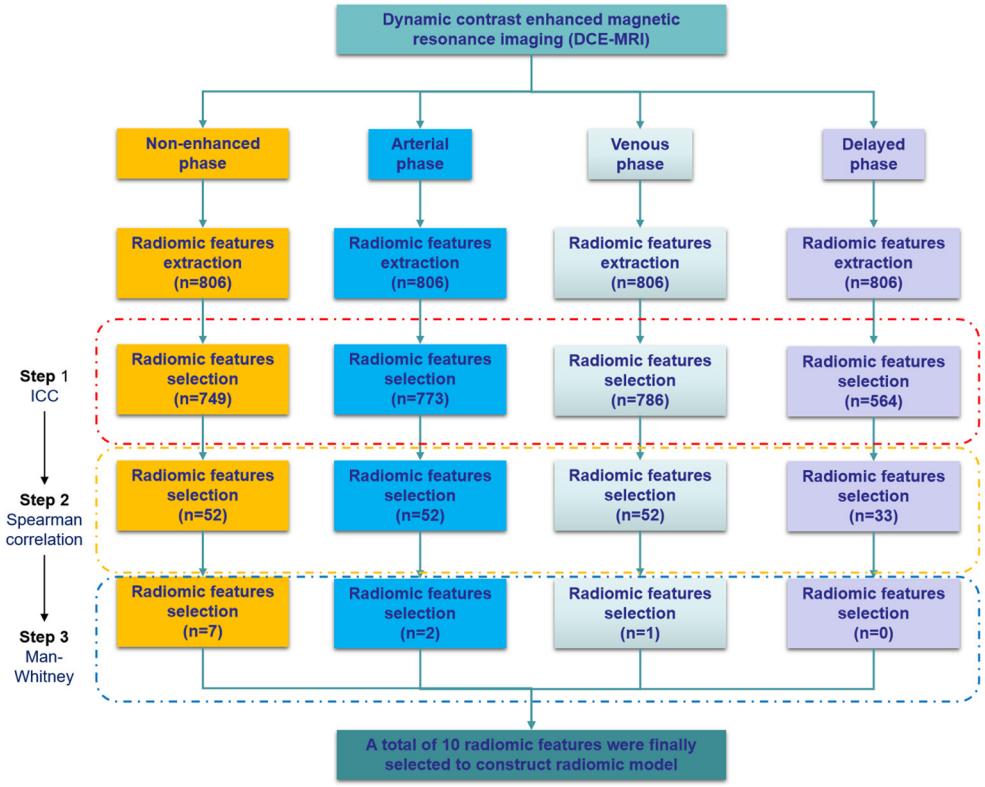

Figure 5. The flowchart of radiomic features extraction, reduction and selection. First, the delineation of VOI in each phase of DCE-MRI for all the included cholangiocarcinoma patients was performed by using 3D Slicer, including the non-enhanced phase, the arterial phase, the venous phase and the delayed phase. Second, a total of 806 radiomic features were generated per lesion in each phase of DCE-MRI for individual cholangiocarcinoma patients. Then, to select the most informative radiomic features to build the radiomic model, three-step radiomic features reduction (ICC analysis, spearman correlation analysis and Man-Whitney *U* test) was performed for each phase of DCE-MRI. In the end, a total of 10 radiomic features from four phases of DEC-MRI were finally selected.

infiltrating $CD3^+$ T ($P < 0.001$), $CD8^+$ T ($P < 0.001$), and $FOXP3^+$ T ($P < 0.001$) were dramatically higher than that in subgroup 2 which represented an immune-cold or immunodeficient subtype (Figure. 4B), suggesting a potential sensitivity to immune checkpoint blockade (ICB) treatment for subgroup 1 but not subgroup 2.

3.3. Extraction and selection of radiomic features derived from DCE-MRI images

Before radiomic features extraction, semiautomatic segmentation by using the 3D Slicer was first performed to delineate the VOI in each phase of dynamic contrast enhancement (DCE) images of MRI, including non-enhanced phase, arterial phase, venous phase and delayed phase. A total of 806 radiomic features were generated per lesion in each phase of DCE-MRI, including shape features ($n = 14$), (b) first-order statistics ($n = 18$), (c) gray-level co-occurrence matrix (GLCM) features ($n = 24$), (d) gray-level dependence matrix (GLDM) features ($n = 14$), (e) gray-level run-length matrix (GLRLM) features ($n = 16$), (f) gray-level size-zone matrix (GLSZM) features ($n = 16$) and wavelet features ($n = 704$). A three-step procedure for radiomic features reduction and selection were utilized to select the most informative radiomic features for immune related subgroup classification for cholangiocarcinoma based on each phase of DCE-MRI, including ICC analysis, spearman correlation analysis and Man-Whitney *U* test. In the end, a total of 10 radiomic features were selected to build the model. The detailed outcome for each radiomic features reduction and selection step is flowcharted in Figure. 5. To illustrate the differences in predictive radiomic features between subgroup 1 and subgroup 2. Representive DCE-MRI images, including the non-enhanced phase, arterial phase and portal venous phase, are presented in Figure. 6. The original DCE-MRI images are shown in Figure. 6A, and the upper row and the lower row is for subgroup 1 and subgroup 2, respectively. The generated images depicting the activities of predictive radomic features within the VOI from representative cholangiocarcinoma patients from subgroup 1 and subgroup 2 are placed in Figure. 6B. As shown, the predictive radiomic feature based on MRI images from non-enhanced phase in subgroup 1 was significantly increased in contrast with that in subgroup 2. Especially, in comparison with subgroup 2, the predicitive radiomic feature based on MRI images from portal venous phase was remarkably enhanced in subgroup 1.

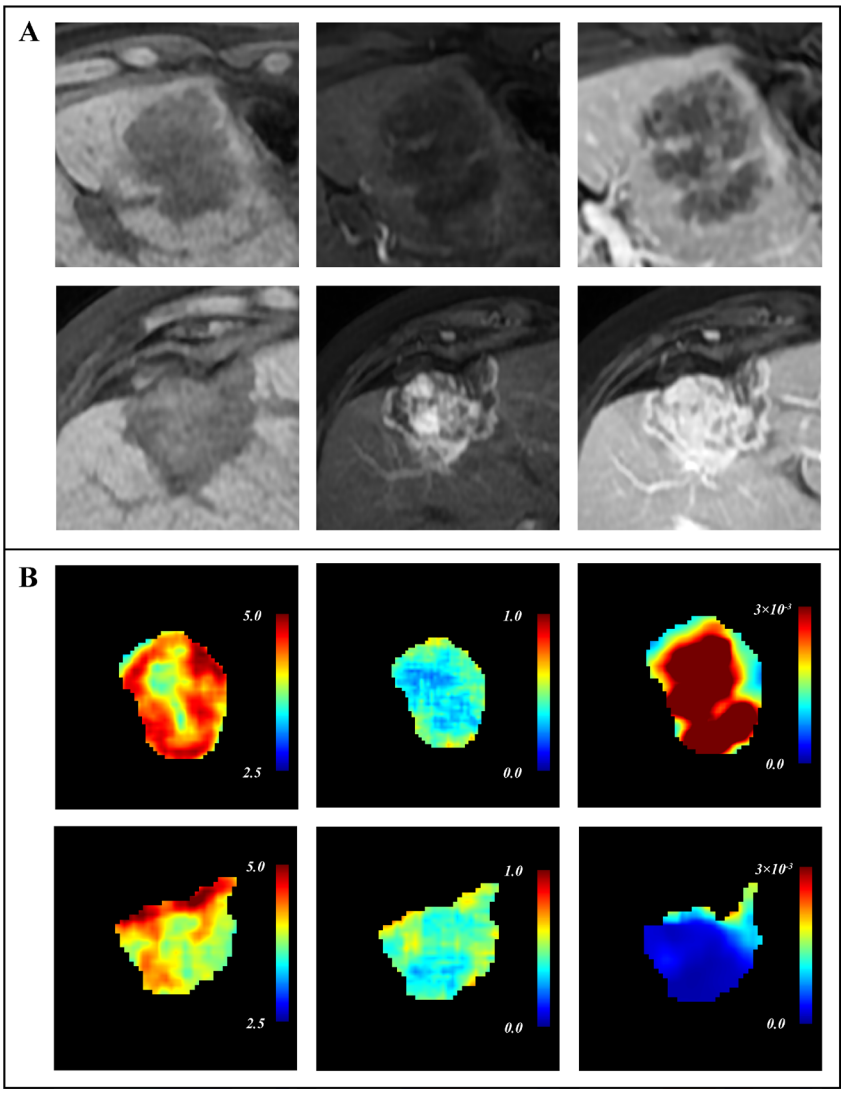

Figure 6. Representative multiple-phase images of DCE-MRI in subgroup 1 and subgroup 2 with pseudo-color delineation of predicitve radiomic features. (**A**) The representative original DCE-MRI images from subgroup 1 (upper) and subgroup 2 (lower). The left column is for the non-enhanced phase, the middle column is for the arterial phase and the right column is for the portal venous phase. (**B**) The generated pseudo-color delineation of predicitve radiomic features within the VOI of representative cholangicarcinoma patients from subgroup 1 and subgroup 2. The left column is for the non-enhanced phase, the middle column is for the arterial phase and the right column is for the portal venous phase.

3.4. The predictive power of the constructed multivariate radiomic model in immune-related subgroup classification for cholangiocarcinoma

A support vector machine with rbf kernel was employed to establish the radiomic model by using the finally selected 10 radiomic features. The ROC curve (Figure. 7A) and the decision curve (Figure. 7B) were drawn to evaluate the predictive power of the developed radiomic model in immune related subgroup classification for cholangiocarcinoma. In order to make the results stable and reliable, three-fold cross-validation was performed and repeated 50 times in the training set. As shown, the mean AUC of the ROC curve for the training set was 0.80 (95% CI 0.64-0.93), with a classification accuracy of 76.47%, a classification sensitivity of 70.59% and a classification specificity of 82.35%. In addition, the 50 prediction results of every patient in the training/validation set based on immune-related subgroup clusteirng were displayed through the violin box diagram (Figure. 7C). As indicated, the predictive probabilities in subgroup 1 were dramatically higher than that in subroup 2 ($P < 0.01$). The stability of this predictive radiomic model was justified by the Chi-Square Goodness-of-Fit test ($\chi^2 = 0.233$, $p = 0.629$) and evaluated by calibration curve analysis which suggested a high level of stability (Figure. 7D).

3.5. The potential clinical translation of the established radiomic model for immunotherapy of cholangiocarcinoma

To test the predictive role of the established radiomic model in immunotherapy for cholangiocarcinoma, a total of 10 cholangiocarcinoma patients who underwent both transcriptome sequencing and ICB treatment after

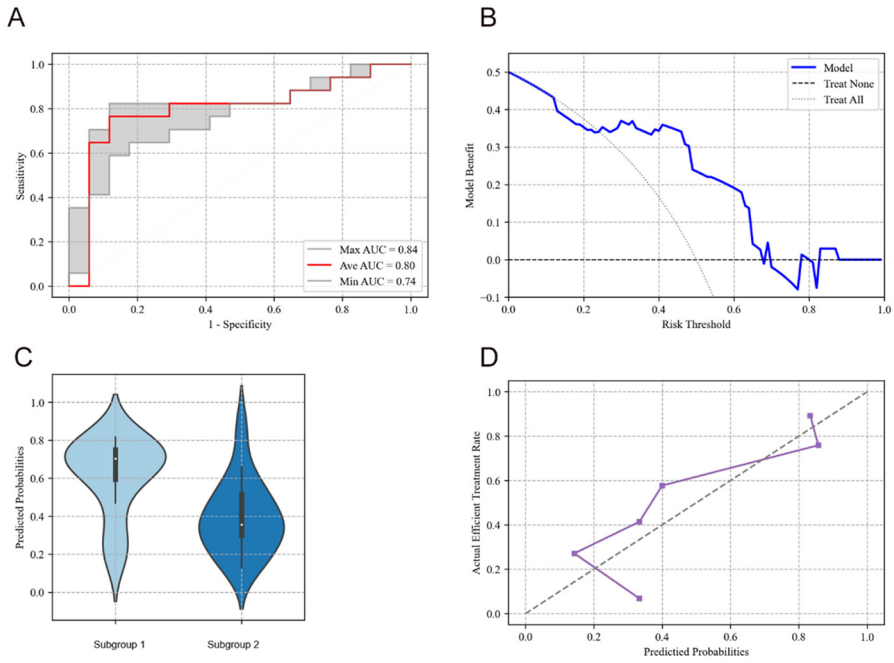

Figure 7. Evaluation of the established radiomic model in prediction of immune-related subgroup classification for cholangiocarcinoma. A ROC curve (**A**) and a decision curve (**B**) were drawn to evaluate the predictive power of the developed radiomic model. (**C**) Moreover, the violin box diagram displayed the distribution of the repeated 50 times predicted probabilities of being recognized as immune-related subgroup 1. (**D**) The stability of this predictive radiomic model was evaluated by calibration curve analysis.

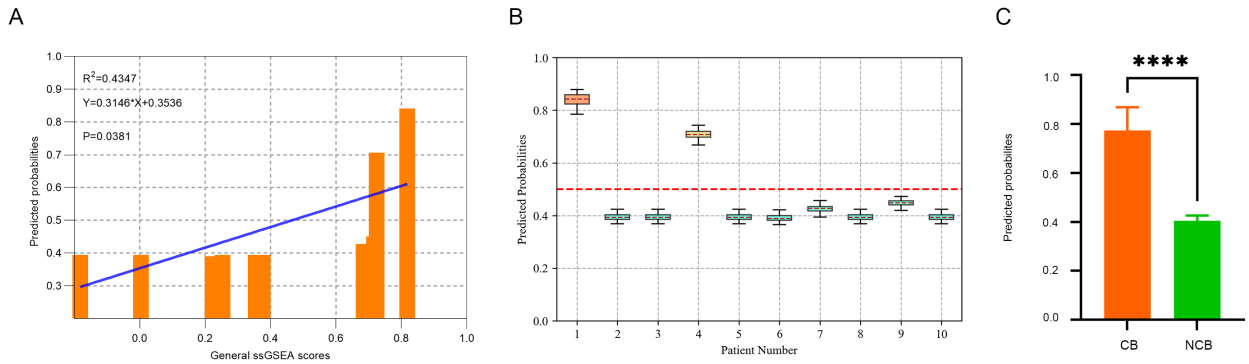

Figure 8. The performance of the established radiomic model in an independent testing cohort. (**A**) As shown in the diagram of regression analysis, the predictive probability of immune-hot subgroup 1 by radiomic model based on DCE-MRI was positively correlated with the immune scores derived from ssGSEA. (**B**) The individual predictive probability to be recognized as immune-hot subgroup 1 for each cholangiocarcinoma patient in the testing cohort (n =10) was calculated by the established radiomic model. (**C**) The relationship between the status of actual response to ICB treatment (CB *vs* NCB) and the predicted probability of being immune-related subgroup 1 for was tested by Mann-Whitney U test.

surgery with complete DCE-MRI information before treatment were included as an independent testing cohort. Regression analysis indicated that the individual probability of being predicted as immune-hot subgroup 1 by radiomics based on DCE-MRI was positively correlated with corresponding individual immune score derived from ssGSEA (Figure. 8A). As exhibited in Figure. 8B, the individual predictive probability of being recognized as immune-hot subgroup 1 for each cholangiocarcinoma patient was calculated by using the established radiomic model. Among the 10 candidates, patients NO.1 and NO.4 with predictive probabilities higher than 0.5 were considered as immune-hot subgroup 1, whereas other patients with predictive probabilities lower than 0.5 were predicted as immune-cold or immune-deficient subgroup 2 (Figure. 8B). Expectedly, based on the actual therapeutic effect evaluation for immunotherapy, patients NO.1 and NO.4 were divided into "clinical benefit (CB)" group who were with partial response (PR). In contrast, other patients were categorized into the "non-clinical benefit (NCB)" group with progressive disease (PD). The relationship between the status of actual response to ICB treatment (CB *vs* NCB) and the predicted probability of being immune-related subgroup 1 for individual cholangiocarcinoma patient was tested by Mann-Whitney U test (Figure. 8C,

$P < 0.0001$), which further verified that the established radiomic signature model was potentially predictive of immunotherapy for cholangiocarcinoma.

4. Discussion

Immunotherapy is emerging as a potentially promising treatment strategy for cholangiocarcinoma (*25*). To further improve the clinical benefit of immunotherapy for cholangiocarcinoma, a noninvasive and accurate selection of potentially responsive patient candidates prior to treatment is urgently required (*26,27*). In the present investigation, an established radiomic signature model based on DCE-MRI was potentially predictive of immune-related subgroup classification for cholangiocarcinoma, allowing for a noninvasive and reliable characterization of local tumor immune landscape to guide immunotherapy for cholangiocarcinoma.

The local immune landscape plays an important role in individualized treatment and precision medicine, particularly for tumor immunotherapy (*5*). On the one hand, characterization of the local tumor immune landscape is needed to guide tumor immunotherapy; On the other hand, a comprehensive and precise determination of tumor immune status is challenging. Currently, immune-related subgroup classification based on transcriptome sequencing is becoming a trend to predict potential reponse to tumor immunotherapy prior to treatment. Especially, distinct immune-associated subtypes in human cholangiocarcinoma (*22,23,28*) and hepatocellular carcinoma (*27*) were reported previously based on sequencing data. In our study, two immune-related subgroups clustering was attained based on tumor mRNA sequencing data through a K-means algorithm, a classical unsupervised learning algorithm of artificial intelligence. These classified two subgroups characterized by different immune landscapes represented potential responder and non-responder to immunotherapy for cholangiocarcinoma, respectively. Multiomic analyses also demonstrated a noticeable advantage of personalized treatment based on TME profiling over molecular targeting therapy based on tumor heterogeneity profiling, considering the more feasibility and the longer-lasting therapeutic effect of the former than the latter (*28-30*). However, similar to IHC assay and flow cytometric assay for tumor immune status determination, transcriptome sequencing was also an invasive approach and dependent on specimen availability. With the development of computing techniques and big data processing algorithms, radiomics and derivative radiogenomics or radiotranscriptomics based on both medical images and sequencing data are emerging as a noninvasive, repetitive and reliable method to reveal the underlying biologcial and molecular mechanism for heterogeneity reflected in radiological features (*31,32*). Though the studies with regard to the biological validation of radiomic findings are increasingly required to conduct, we have to keep in mind that the level of biological insight and analytical tools used in genomics or transcriptomics are largely not available for radiomics. As the field of radiomics grows, more and more relationships between radiomic features and radiomic meaning are being revealed, and a relevant database platform is expected to establish.

In the study, a large amount of radiomic features captured in the DCE-MRI images were extracted and selected to build a multivariate radiomic signature model to predict immune-related subgroup classification. As shown in the results of ROC analysis, the constructed radiomic signature model was able to discriminate between different immune-related subgroups with an AUC of up to 0.80. Among the finally selected 10 radiomic features for construction of the predictive model in the study, five of them were from original texture features, whereas the other five were from wavelet radiomic features. Additionally, the selected radiomic features consist of 7 from the non-enhanced phase, 2 from the arterial phase and 1 from the venous phase. Consistently, it was found that the predictive radiomic signature was mainly composed by maximum, median, entropy, kurtosis, emphasis, correlation and non-uniformity. All of these features contributed to reflect the heterogeneity captured in the DCE-MRI images from different aspects, suggesting that the established radiomic model was capable of predicting the immune status in TME by quantitively characterizing heterogeneity reflected in the DCE-MRI images. Although predictive radiomic models based on MRI for immunotherapy were already previously reported for several types of cancer, such as breast cancer (*33*), MRI-derived radiomics with regard to immunotherapy for cholangiocarcinoma was rare. Though investigations conducted by Zhang *et als* (*18,19*) mainly focused on the relationship between MRI-derived radiomic signature and immunophenotyping and survival for cholangiocarcinoma, only the status of PD-1/PD-L1 status and $CD8^+$ T cells infiltration were determined to represent the immune profile for cholangiocarcinoma. However, patient clustering based on a comprehensive characterization of the TME to perform subsequent radiomic analysis needs to be improved in their studies. In the present study, radiotranscriptomics but not radiomics was performed to identify the potential association between tumor immune profile and developed radiomic signature model based on MRI for cholangiocarcinoma. Study from Wang *et al*. (*34*) also revealed a link between radiomic biomarker and TME in breast cancer, consistent with our investigation. However, only MRI images from one single phase, usually arterial phase, were commonly used to establish radiomic signature model by previous investigations (*17,18*). The radiomic model developed in our study was based on four phase images of DCE-MRI. Presumably, multi-phase DCE-MRI radiomics was able to provide more information about heterogeneity in TME in contrast with radiomics from single-phase images. As reported by

Li *et al*., machine learning based on multi-phase images, DCE-MRI outperformed single-phase MRI in early prediction of pathological complete response (pCR) to neoadjuvant therapy (NAT) in human epithelial growth factor receptor 2 (HER2) positive invasive breast cancer (*35*).

Noticeably, an independent testing cohort of cholangiocarcinoma patients with immunotherapy who underwent both tumor transcriptome sequencing and DCE-MRI examination prior to treatment were also enrolled in the study to validate the predictive power of the constructed radiomic signature model in immunotherapy for cholangiocarcinoma. As shown, the significant relationship between the predictive probability of being immune-related subgroup 1 by this established model and actual therapeutic response state to immunotherapy highly suggested the capacity of this model to effectively predict immunotherapy for cholangiocarcinoma.

Apart from MRI-derived radiomics, artificial intelligence (AI) techniques based on other clinical imaging modalities were also helpful to tumor immunotherapy, especially for ^{18}F-Fluorodeoxyglucose positron emission tomography/computed tomography (^{18}F-FDG PET/CT) imaging (*36,37*). As known, both attenuated tumor immunity and tumor metabolic reprogramming, which are also intimately correlated, are important hallmarks of tumor (*38,39*). In our previous work, immunosuppression in HCC could be induced by metabolic modulation (*40*). Accordingly, ^{18}F-FDG PET images, which could provide metabolic information in tumors, is promisingly predictive of the immune profile in TME and potentially applied in tumor immunotherapy. Consistently, PET-derived radiomics was also reported to be able to reveal transcriptomics in cancer (*41*). Furthermore, the predictive roles of AI analysis based on PET/CT images in immune profiling, immunotherapy response and survival for NSCLC were suggested by previous investigations (*42,43*). With the development of immuno-PET techniques and AI techniques, direct integration of them is expected to accurately predict tumor immunotherapy (*44,45*).

Despite the encouraging results in this study, several limitations in the current work need to be addressed. First, only cholangiocarcinoma patients with preoperative DCE-MRI and postoperative transcriptome sequencing and IHC staining for immune cell infiltration were included, which resulted in a limitied sample size for radiomic analysis. However, this primary radiotranscriptomic analysis shed light on the biological validation of established predictive radiomic models for immunotherapy in cholangiocarcinoma, because relevant investigation is rare due to the lack of simultaneous collection of imaging data and tumor mRNA sequencing data for cholangiocarcinoma from other research groups and public database, such as the Cancer Genome Atlas (TCGA) with imaging information from The cancer Imaging Archive (TCIA). Additionally, the potential overfitting of this predictive radiomic model was prevented by cross-validation with repetition for 50 times and inclusion of an independent testing cohort, and the analytical results from both the Chi-Square Goodness-of-Fit test and calibration curve analysis suggested a low likelihood of overfitting for this model. For sure, a prospective trial in the near future is needed to verify the results; Second, limited by the small sample size of this single-center study, a further study with a larger training cohort and external test cohorts from multi-center was warranted to confirm the conclusion obtained in the work. Then, TILs representation in cholangiocarcinoma specimens was only evaluated by IHC assay, an immunologic function assay was not performed to analyze the functional status of immune cells in local TME. With a sufficient size of specimen, cytometric analyses based on fresh isolation of TILs from tissue samples would partially address this issue. In the end, a comprehensive model involving both radiomic features and clinicopathological parameters was expected to develop to noninvasively predict the response probability to immunotherapy for cholangiocarcinoma.

5. Conclusion

The local tumor immune microenvironment is increasingly accepted as a vital factor influencing the sensitivity and outcome of tumor immunotherapy. Thus, characterization of the immune status in TME prior to tumor immunotherapy allows for the selection of potentially responsive candidates who would benefit from immunotherapy. An immune-related subgroup classification based on RNA sequencing data is capable of providing comprehensive information for immune profiling in cholangiocarcinoma. Furthermore, the developed radiomic model based on DCE-MRI in the study is potentially applied as a noninvasive, repetitive and reliable approach to predict the immune-related subgroup classification and response probability to immunotherapy for cholangiocarcinoma.

Funding: This work was supported by a grant from the national natural science foundation of China (grant nos. 82272074, 82373365), the natural science foundation of our city (21JCQNJC01290), the health science and technology project in our city (TJWJ2022MS008), the key medical discipline (Pathology) construction project in our city (TJYXZDXK-012A), the Key Medical Discipline (Specialty) construction project (TJYXZDXK-009A) and the accurate diagnosis of tumor and pharmacotherapy technology construction project in our institution (grant nos. ZLJZZDYYWZL11 and ZLJZZDYYWZL03).

Conflict of Interest: The authors have no conflicts of interest to disclose.

References

1. Bray F, Ferlay J, Soerjomataram I, Siegel RL, Torre LA, Jemal A. Global cancer statistics 2018: GLOBOCAN estimates of incidence and mortality worldwide for 36 cancers in 185 countries. CA Cancer J Clin. 2018; 68:394-424.
2. Siegel RL, Miller KD, Fuchs HE, Jemal A. Cancer Statistics, 2021. CA Cancer J Clin. 2021; 71:7-33.
3. Bridgewater J, Galle PR, Khan SA, Llovet JM, Park JW, Patel T, Pawlik TM, Gores GJ. Guidelines for the diagnosis and management of intrahepatic cholangiocarcinoma. J Hepatol. 2014; 60:1268-1289.
4. Rizvi S, Khan SA, Hallemeier CL, Kelley RK, Gores GJ. Cholangiocarcinoma-evolving concepts and therapeutic strategies. Nat Rev Clin Oncol. 2018; 15:95-111.
5. Sadeghi Rad H, Monkman J, Warkiani ME, Ladwa R, O'Byrne K, Rezaei N, Kulasinghe A. Understanding the tumor microenvironment for effective immunotherapy. Med Res Rev. 2021; 41:1474-98.
6. Charalampakis N, Papageorgiou G, Tsakatikas S, Fioretzaki R, Kole C, Kykalos S, Tolia M, Schizas D. Immunotherapy for cholangiocarcinoma: A 2021 update. Immunotherapy. 2021; 13:1113-1134.
7. Al-Rajabi R, Sun W. Immunotherapy in cholangiocarcinoma. Curr Opin Gastroenterol. 2021; 37:105-111.
8. Carlino MS, Larkin J, Long GV. Immune checkpoint inhibitors in melanoma. Lancet. 2021; 398:1002-1014.
9. Kline J, Godfrey J, Ansell SM. The immune landscape and response to immune checkpoint blockade therapy in lymphoma. Blood. 2020; 135:523-533.
10. Lin A, Wei T, Meng H, Luo P, Zhang J. Role of the dynamic tumor microenvironment in controversies regarding immune checkpoint inhibitors for the treatment of non-small cell lung cancer (NSCLC) with EGFR mutations. Mol Cancer. 2019; 18:139.
11. Bashash D, Zandi Z, Kashani B, Pourbagheri-Sigaroodi A, Salari S, Ghaffari SH. Resistance to immunotherapy in human malignancies: Mechanisms, research progresses, challenges, and opportunities. J Cell Physiol. 2022; 237:346-372.
12. Gibney GT, Weiner LM, Atkins MB. Predictive biomarkers for checkpoint inhibitor-based immunotherapy. Lancet Oncol. 2016; 17:e542-e551.
13. Ren D, Hua Y, Yu B, *et al*. Predictive biomarkers and mechanisms underlying resistance to PD1/PD-L1 blockade cancer immunotherapy. Mol Cancer. 2020; 19:19.
14. Paijens ST, Vledder A, de Bruyn M, Nijman HW. Tumor-infiltrating lymphocytes in the immunotherapy era. Cell Mol Immunol. 2021; 18:842-859.
15. Patel SP, Kurzrock R. PD-L1 Expression as a Predictive Biomarker in Cancer Immunotherapy. Mol Cancer Ther. 2015; 14:847-856.
16. Xia T, Li K, Niu N, *et al*. Immune cell atlas of cholangiocarcinomas reveals distinct tumor microenvironments and associated prognoses. J Hematol Oncol. 2022; 15:37.
17. Min JH, Kim YK, Choi SY, Kang TW, Lee SJ, Kim JM, Ahn S, Cho H. Intrahepatic Mass-forming Cholangiocarcinoma: Arterial Enhancement Patterns at MRI and Prognosis. Radiology. 2019; 290(3):691-699.
18. Zhang J, Wu Z, Zhao J, Liu S, Zhang X, Yuan F, Shi Y, Song B. Intrahepatic cholangiocarcinoma: MRI texture signature as predictive biomarkers of immunophenotyping and survival. Eur Radiol. 2021; 31:3661-3672.
19. Zhang J, Wu Z, Zhang X, Liu S, Zhao J, Yuan F, Shi Y, Song B. Machine learning: an approach to preoperatively predict PD-1/PD-L1 expression and outcome in intrahepatic cholangiocarcinoma using MRI biomarkers. ESMO Open. 2020; 5:e000910.
20. Mayerhoefer ME, Materka A, Langs G, Häggström I, Szczypiński P, Gibbs P, Cook G. Introduction to Radiomics. J Nucl Med. 2020; 61:488-495.
21. Job S, Rapoud D, Dos Santos A, *et al*. Identification of Four Immune Subtypes Characterized by Distinct Composition and Functions of Tumor Microenvironment in Intrahepatic Cholangiocarcinoma. Hepatology. 2020; 72:965-981.
22. Huang X, Tang T, Zhang G, Liang T. Identification of tumor antigens and immune subtypes of cholangiocarcinoma for mRNA vaccine development. Mol Cancer. 2021; 20:50.
23. Li S, Xu F, Li H, Zhang J, Zhong A, Huang B, Lai M. S100A8+ stroma cells predict a good prognosis and inhibit aggressiveness in colorectal carcinoma. Oncoimmunology. 2016; 6:e1260213.
24. Fiste O, Ntanasis-Stathopoulos I, Gavriatopoulou M, Liontos M, Koutsoukos K, Dimopoulos MA, Zagouri F. The Emerging Role of Immunotherapy in Intrahepatic Cholangiocarcinoma. Vaccines (Basel). 2021; 9:422.
25. Du Y, Qi Y, Jin Z, Tian J. Noninvasive imaging in cancer immunotherapy: The way to precision medicine. Cancer Lett. 2019; 466:13-22.
26. Deutsch E, Paragios N. Radiomics to predict response to immunotherapy, bridging the gap from proof of concept to clinical applicability? Ann Oncol. 2019; 30:879-881.
27. Chen S, Xie Y, Cai Y, *et al*. Multiomic Analysis Reveals Comprehensive Tumor Heterogeneity and Distinct Immune Subtypes in Multifocal Intrahepatic Cholangiocarcinoma. Clin Cancer Res. 2022; 28:1896-1910.
28. Ho DW, Tsui YM, Chan LK, *et al*. Single-cell RNA sequencing shows the immunosuppressive landscape and tumor heterogeneity of HBV-associated hepatocellular carcinoma. Nat Commun. 2021; 12:3684.
29. Zhang Q, Lou Y, Yang J, *et al*. Integrated multiomic analysis reveals comprehensive tumour heterogeneity and novel immunophenotypic classification in hepatocellular carcinomas. Gut. 2019; 68:2019-2031.
30. Martin-Serrano MA, Kepecs B, Torres-Martin M, *et al*. Novel microenvironment-based classification of intrahepatic cholangiocarcinoma with therapeutic implications. Gut. 2023; 72:736-748.
31. Jeong WK, Jamshidi N, Felker ER, Raman SS, Lu DS. Radiomics and radiogenomics of primary liver cancers. Clin Mol Hepatol. 2019; 25:21-29.
32. Saini A, Breen I, Pershad Y, Naidu S. Radiogenomics and Radiomics in Liver Cancers. Diagnostics (Basel). 2018; 9:4.
33. Bian T, Wu Z, Lin Q, Mao Y, Wang H, Chen J, Chen Q, Fu G, Cui C, Su X. Evaluating Tumor-Infiltrating Lymphocytes in Breast Cancer Using Preoperative MRI-Based Radiomics. J Magn Reson Imaging. 2022; 55:772-784.
34. Wang X, Xie T, Luo J, Zhou Z, Yu X, Guo X. Radiomics predicts the prognosis of patients with locally advanced breast cancer by reflecting the heterogeneity of tumor

cells and the tumor microenvironment. Breast Cancer Res. 2022; 24:20.
35. Li Q, Xiao Q, Li J, Wang Z, Wang H, Gu Y. Value of Machine Learning with Multiphases CE-MRI Radiomics for Early Prediction of Pathological Complete Response to Neoadjuvant Therapy in HER2-Positive Invasive Breast Cancer. Cancer Manag Res. 2021; 13:5053-5062.
36. Mu W, Tunali I, Gray JE, Qi J, Schabath MB, Gillies RJ. Radiomics of 18F-FDG PET/CT images predicts clinical benefit of advanced NSCLC patients to checkpoint blockade immunotherapy. Eur J Nucl Med Mol Imaging. 2020; 47:1168-1182.
37. Mu W, Jiang L, Shi Y, Tunali I, Gray JE, Katsoulakis E, Tian J, Gillies RJ, Schabath MB. Non-invasive measurement of PD-L1 status and prediction of immunotherapy response using deep learning of PET/CT images. J Immunother Cancer. 2021; 9:e002118.
38. RRenner K, Singer K, Koehl GE, Geissler EK, Peter K, Siska PJ, Kreutz M. Metabolic Hallmarks of Tumor and Immune Cells in the Tumor Microenvironment. Front Immunol. 2017; 8:248.
39. Bader JE, Voss K, Rathmell JC. Targeting Metabolism to Improve the Tumor Microenvironment for Cancer Immunotherapy. Mol Cell. 2020; 78:1019-1033.
40. Li X, Zhang Y, Ma W, Fu Q, Liu J, Yin G, Chen P, Dai D, Chen W, Qi L, Yu X, Xu W. Enhanced glucose metabolism mediated by CD147 contributes to immunosuppression in hepatocellular carcinoma. Cancer Immunol Immunother. 2020; 69:535-548.
41. Tixier F, Cheze-le-Rest C, Schick U, Simon B, Dufour X, Key S, Pradier O, Aubry M, Hatt M, Corcos L, Visvikis D. Transcriptomics in cancer revealed by Positron Emission Tomography radiomics. Sci Rep. 2020; 10:5660.
42. Polverari G, Ceci F, Bertaglia V, Reale ML, Rampado O, Gallio E, Passera R, Liberini V, Scapoli P, Arena V, Racca M, Veltri A, Novello S, Deandreis D. 18F-FDG Pet Parameters and Radiomics Features Analysis in Advanced Nsclc Treated with Immunotherapy as Predictors of Therapy Response and Survival. Cancers (Basel). 2020; 12:1163.
43. Tong H, Sun J, Fang J, Zhang M, Liu H, Xia R, Zhou W, Liu K, Chen X. A Machine Learning Model Based on PET/CT Radiomics and Clinical Characteristics Predicts Tumor Immune Profiles in Non-Small Cell Lung Cancer: A Retrospective Multicohort Study. Front Immunol. 2022; 13:859323.
44. Liberini V, Laudicella R, Capozza M, Huellner MW, Burger IA, Baldari S, Terreno E, Deandreis D. The Future of Cancer Diagnosis, Treatment and Surveillance: A Systemic Review on Immunotherapy and Immuno-PET Radiotracers. Molecules. 2021; 26:2201.
45. Dercle L, Sun S, Seban RD, *et al*. Emerging and Evolving Concepts in Cancer Immunotherapy Imaging. Radiology. 2023; 306:32-46.

Received May 8, 2024; Revised June 7, 2024; Accepted June 9, 2024.

[§]These authors contributed equally to this work.
**Address correspondence to:*
Xiaofeng Li and Lisha Qi, Tianjin Medical University Cancer Institute and Hospital, Huan-Hu-Xi Road, Ti-Yuan-Bei, He Xi District, Tianjin 300060, PR China.
E-mail: Xli03@tmu.edu.cn (Xiaofeng Li); Lqi01@tmu.edu.cn (Lisha Qi)

Released online in J-STAGE as advance publication June 10, 2024.